ADVANCED FUNCTIONAL MATERIALS
www.afm-journal.de

Relating the Physical Structure and Optoelectronic Function of Crystalline TIPS-Pentacene

Sahar Sharifzadeh, Cathy Y. Wong, Hao Wu, Benjamin L. Cotts, Leeor Kronik, Naomi S. Ginsberg, and Jeffrey B. Neaton**

Theory and experiment are combined to investigate the nature of low-energy excitons within ordered domains of 6,13-bis(triisopropylsilylethynyl)-pentacene (TIPS-PEN) polycrystalline thin films. First-principles density functional theory and many-body perturbation theory calculations, along with polarization-dependent optical absorption spectro-microscopy on ordered domains, show multiple low-energy absorption peaks that are composed of excitonic states delocalized over several molecules. While the first absorption peak is composed of a single excitonic transition and retains the polarization-dependent behavior of the molecule, higher energy peaks are composed of multiple transitions with optical properties that can not be described by those of the molecule. The predicted structure-dependence of polarization-dependent absorption reveals the exact inter-grain orientation within the TIPS-PEN film. Additionally, the degree of exciton delocalization can be significantly tuned by modest changes in the solid-state structure and the spatial extent of the excitations along a given direction is correlated with the degree of electronic dispersion along the same direction. These findings pave the way for tailoring the singlet fission efficiency of organic crystals by solid-state structure.

1. Introduction

Organic semiconductors are a highly tunable class of inexpensive, easily processable, and optically active materials that are promising for next-generation photovoltaics and other optoelectronics applications. While many organic materials have varying degrees of disorder, crystalline films with long-range order provide an opportunity to understand many fundamental physical properties relevant to solar energy conversion. Additionally, organic crystals are promising in their own right due to the efficient carrier and energy transport properties associated with their long-range order.

In particular, crystalline and polycrystalline films of pentacene (PEN) and its derivatives have high carrier mobility for charge transport (≈1–10 cm^2/Vs hole mobility)[1] and significant photoconductivity.[2,3] Moreover, PEN and many of its derivatives display a propensity for singlet fission (SF),[4,5] a phenomenon that results in greater than 100% internal quantum efficiency in organic photovoltaics. Numerous possible molecular functionalizations may modify solid-state structural and optoelectronic properties.[6] Therefore, elucidating the structure-property relation is important for the design of new functional molecular materials.

6,13-bis(triisopropylsilylethynyl)-pentacene (TIPS-PEN),[7] shown in **Figure 1**, has recently attracted much interest. The bulky groups functionalizing PEN enable solubility in organic solvents and allow for solution-processing of polycrystalline TIPS-PEN thin films with high carrier mobility and photoconductivity.[2,3,7] While TIPS-PEN apparently retains optical properties similar to PEN, its enhanced carrier mobility[8] and

Prof. S. Sharifzadeh
Molecular Foundry
Lawrence Berkeley National Laboratory
Berkeley, CA, 94720, USA
E-mail: ssharifz@bu.edu; jbneaton@lbl.gov
Prof. S. Sharifzadeh
Department of Electrical and Computer Engineering
Boston University
Boston, MA, 02215, USA
Prof. S. Sharifzadeh
Materials Science and Engineering Division
Boston University
Boston, MA, 02215, USA
Dr. C. Y. Wong, H. Wu, B. L. Cotts, Prof. N. S. Ginsberg
Department of Chemistry
University of California, Berkeley
Berkeley, CA, 94720, US

DOI: 10.1002/adfm.201403005

Prof. L. Kronik
Department of Materials and Interfaces
Weizmann Institute of Science
Rehovoth, 76100, Israel
Prof. N. S. Ginsberg
Physical Biosciences Division
Lawrence Berkeley National Laboratory
Berkeley, CA, 94720, USA
Prof. N. S. Ginsberg, Prof. J. B. Neaton
Department of Physics
University of California Berkeley
Berkeley, CA, 94720, USA
Prof. N. S. Ginsberg, Prof. J. B. Neaton
Kavli Energy NanoSciences Institute at Berkeley
Berkeley, CA, 94720, USA
Prof. N. S. Ginsberg, Prof. J. B. Neaton
Materials Sciences Division
Lawrence Berkeley National Laboratory
Berkeley, CA, 94720, CA

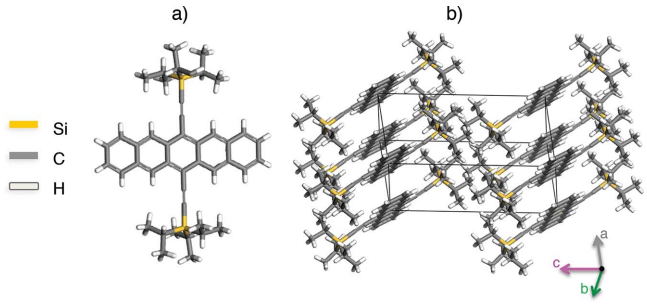

Figure 1. a) Gas-phase molecule and b) bulk triclinic single-crystal structure of TIPS-PEN.[7] For the gas-phase molecule, we use the standard notation such that the long-axis is along the aromatic backbone and the short axis is perpendicular, connecting the functional groups. The **a**,**b**,**c** crystallographic axes are as indicated in the figure.

increased air stability[9] additionally improve its applicability as an optoelectronic material. Importantly, the inter-molecular structure of TIPS-PEN films is highly tunable via changes in growth conditions, allowing for ready modification of charge mobility[7,10,11] and SF efficiency.[12–15]

TIPS-PEN molecules crystallize in a brick-layer-type crystalline structure with adjacent molecules staggered in a face-to-face manner;[7] in contrast, PEN condenses in a herringbone face-to-edge arrangement.[16] The brick-layer-type structure of TIPS-PEN leads to a different degree and nature of π-orbital overlap, resulting in direction-dependent carrier mobilities[17,18] and distinct solid-state electrostatics[19] relative to PEN. The nature of low-lying singlet and triplet excitations (i.e., excitons) in TIPS-PEN, however, has yet to be determined.

In this study, we investigate the role of solid-state structure on the excitonic properties of crystalline TIPS-PEN using spatially-resolved polarization-dependent linear optical absorption measurements, as well as ab initio density functional theory (DFT) and many-body perturbation theory (MBPT). Previous DFT-based studies of the optical absorption of TIPS-PEN have focused on deriving information about the extended crystal from calculations of finite systems such as the dimer[20] or from finite-sized cluster.[19] Here, we report new insight from what we believe to be the first calculations on the extended crystal. MBPT within the GW approximation and Bethe Salpeter equation (BSE) approach, a well-established methodology employed in prior work to successfully predict optical properties of the PEN molecule and crystal (e.g., Refs.[21–25]) is used to quantitatively explain experimental observations of polarization-dependent optical absorption and to provide physical insight into the excited states of TIPS-PEN. Our computed optical absorption spectrum indicates that the different peaks in the optical absorption spectrum are composed of multiple excitonic transitions. Moreover, a spectro-microscopic approach is used to experimentally probe the optical properties of single crystalline domains within polycrystalline films.[26] Spatially-resolved polarization angle-dependent absorption measurements reveal that individual grains within the polycrystalline film have the same crystal structure but different relative orientation. Our quantitative calculations elucidate the relationship between the polarization-dependence of the absorption and the solid-state structure, allowing the determination of the relative orientation of an arbitrary pair of adjacent grains. Lastly, we analyze the two-particle wavefunctions of low-lying singlets to elucidate their spatial extent and anisotropy. We predict that, at zero temperature, the spatial distribution of the four lowest energy singlet excitons (at 1.7–1.8 eV) is quasi two-dimensional and largely confined to the *ab* plane, with a delocalization length of ≈3–6 molecules along directions of π-orbital stacking, which is correlated with band dispersion along these directions. These calculations demonstrate that both short-range molecular and long-range solid-state effects significantly influence the optical properties of crystalline TIPS-PEN.

2. Experimental Section

Experiment: All measurements are performed on samples consisting of TIPS-PEN molecules supplied by Aldrich and used without further purification to prepare a 5 mg/mL solution in toluene. As described elsewhere,[26] this solution is filtered (0.2 µm pore size) and dropcast onto clean glass substrates on top of a hot plate held at ≈60 °C. To control the evaporation rate, samples are covered with a petri dish after deposition, yielding ≈600 nm-thick films with fingerlike domains 10–150 µm wide and up to hundreds of µm long. Samples are then mounted face down onto large rectangular coverslips and bulk linear absorption spectra are collected using a Cary 100 UV-Vis spectrophotometer. To perform polarized linear absorption measurements, light from a tungsten lamp passing through the monochromator of a Perkin Elmer Lambda 800 spectrometer is collimated and directed into a homebuilt optical microscope. A polarizer is placed in the beam path to eliminate any polarization effects introduced by the grating monochromator, and a half-waveplate in a computer-controlled motorized rotation mount (Newport) is placed after the polarizer to control the polarization of the light incident on the sample. This linearly polarized light is directed through a 0.4 NA 10X Plan Apo Leica objective onto the sample. The transmitted light is then collected using an identical objective and imaged onto a CMOS camera (Thorlabs DCC1545M). Using 10 degree polarization increments and 4 nm wavelength increments, wide field transmission images are collected from the sample and from a blank microscope slide, enabling the determination of absorption as a function of position within the field of view, light polarization, and wavelength.

Computation: First-principles many-body perturbation theory calculations are performed using the BerkeleyGW package,[27] with the computational details following previous work.[23,24] In short, we compute quasiparticle excitation energies via the GW approximation,[28] as a first-order correction to a density functional theory (DFT) starting point, within the generalized gradient approximation of Perdew, Burke, and Ernzerhof (PBE),[29] and optical excitations by explicit inclusion of electron-hole interactions, via a BSE approach.[30] DFT-PBE calculations are performed using the Quantum Espresso package which utilizes a planewave basis.[31] Nuclei and core electrons are described by Troullier-Martins norm-conserving pseudopotentials[32] built using the default settings within the Quantum Espresso Pseudopotential Library.[33] Here, 1, 4, and 4 electrons are explicitly considered as valence electrons for H, C, and Si, respectively, and the core cutoff radii are 0.5, 1.3, and 1.8 a.u,

respectively. The planewave energy cutoff for the DFT calculations is 1088 eV and the Kohn-Sham orbitals of the crystal are expanded in a k-point mesh of 4 × 4 × 2, sufficient to converge the near-gap Kohn-Sham orbital energies to 0.1 meV. The molecular geometries for both the gas- and crystalline- phases are optimized within DFT-PBE. For computational convenience, calculations on the gas-phase molecule do not include the methyl side groups attached to Si. This is an acceptable approximation for the low-energy excitations of the molecule because we predict that within DFT-PBE, the frontier π-type molecular orbitals of TIPS-PEN do not extend beyond the Si atom. The methyl groups are included for all solid-state calculations. Additionally, because DFT-PBE does not capture weak dispersion forces that dominate the inter-molecular interactions within the crystal, the lattice vectors are set to the measured bulk values in our calculations. TIPS-PEN crystallizes in a triclinic, $P\bar{1}$ structure, with a slightly different thin-film and bulk single crystal structure.[7,11,34] We expect that the latter will be prevalent in the majority of our films owing to their thickness. The bulk primitive cell used here contains one molecule and has the following lattice parameters: a = 15.39 Å, b = 15.66 Å, c = 16.79 Å, A = 103.5°, β = 88.0°, and γ = 99.0°.[7] All intra-molecular distances are optimized within DFT-PBE. For our GW calculations, we take a "one-shot" G_0W_0@PBE approach: the quasiparticle wavefunctions are assumed to be well-approximated by the DFT-PBE Kohn-Sham states and the energies of these states are corrected perturbatively. The total number of states used to build the dielectric function and self-energy are 4992 and 792 for molecule and solid, respectively, spanning an energy range > 35 eV above the highest occupied state. The dielectric function planewave cutoff is 160 eV. Previous studies of prototypical organic semiconductors found that these parameters converged energy differences of near-gap states to ≈0.02 eV.[23] To avoid spurious interactions with periodic images, the gas-phase molecule is placed in a supercell with lattice vectors twice the size necessary to contain 99% of the charge density and the Coulomb interaction is truncated at distances larger than half of the unit cell size. The supercell dimensions are 59 × 60 × 20 a.u. for the gas-phase TIPS-PEN. Subsequent to our GW calculations, the BSE is solved within the Tamm-Dancoff and static approximations;[30] with information from the solution of the BSE, we further compute the complex macroscopic transverse dielectric function, $\epsilon(\omega) = \epsilon_1(\omega) + i\epsilon_2(\omega)$. This function is related to the absorption coefficient, $\alpha(\omega)$ via the standard expression[35]

$$\alpha(\omega) = 2\omega\sqrt{1/2[-\epsilon_1(\omega) + \sqrt{\epsilon_1(\omega)^2 + \epsilon_2(\omega)^2}]} \quad (1)$$

where ω has units of energy (in atomic units). Additionally, we compute the exciton wavefunction, $\psi(\mathbf{r}_e, \mathbf{r}_h)$, from the BSE as a linear combination of single excitations from the ground state, where one electron is promoted from an occupied to an unoccupied state, and evaluate its spatial extent and distribution via an electron-hole correlation function, $\mathcal{F}(\mathbf{r})$. As defined previously,[24] $\mathcal{F}(\mathbf{r})$ is the probability of finding electron and hole separated by a vector $\mathbf{r}$ as

$$\mathcal{F}(\mathbf{r}) = \int_{\Omega} d^3\mathbf{r}_h \left|\psi(\mathbf{r}_e = \mathbf{r}_h + \mathbf{r}, \mathbf{r}_h)\right|^2 \quad (2)$$

where $\mathbf{r}_e$ and $\mathbf{r}_h$ are the electron and hole coordinates, respectively, and Ω is the volume of a primitive cell.[36–38] As noted recently,[24,39] an electron-hole correlation function is convenient for understanding the nature of the exciton within centrosymmetric organic crystals. We note that even though the calculations are performed in a periodic system, $\mathcal{F}(\mathbf{r})$ is not periodic because the unit cell is expanded in a supercell via **k**-point sampling. Each quasiparticle wavefunction is lattice periodic; however, $\psi(\mathbf{r}_e, \mathbf{r}_h)$ is constructed as a summation of electron-hole pairs with different wavevectors $\boldsymbol{k}$ and $\boldsymbol{k}$', resulting in an electron-hole correlation function that is not periodic. Our BSE calculations include 14 occupied and 14 unoccupied bands for both the gas-phase molecule and solid; parameters that converge the energy of the first four singlet excited-states in the gas- and crystalline- phase to within 0.01 eV. For the solid, a real space 14 × 14 × 6 supercell is used to obtain convergence of exciton wavefunctions and correlation functions. To compare with measurements on thin films, we calculate $\epsilon_2(\omega)$ and $\alpha(\omega)$ from Equation 1 for 18 different polarization directions within the crystal. The polarization direction is systematically varied stepwise by 10 degrees within the *ab* plane, going from the **a** axis to the **-a** axis. For very thin TIPS-PEN polycrystalline films, the molecules crystallize with the *ab* plane parallel to the plane of the substrate.[40] We assume that this is also the case for the films in this study and that the light incident on the sample is normal to this plane. Therefore, the light polarization is varied only within this plane. In order to reduce computational cost, the transition dipole is computed via the momentum operator, which does not account for the contribution of the non-local component of the norm-conserving pseudopotential to the oscillator strengths.[30] We tested the accuracy of this approach for obtaining ϵ_2 against the use of the velocity operator, which correctly describes the influence of the pseudopotential, for the case of light polarized along the **a** and **b** axes and found no significant difference. We compute the integral in Equation 2 as a discrete sum over $\mathbf{r}_h$, with the hole sampled at 7 high hole probability positions on one molecule within the 14 × 14 × 6 supercell. These positions are ≈0.5 Å above the plane of the PEN backbone at each symmetry inequivalent carbon atom. For each hole position, $\mathcal{F}(\mathbf{r})$ is computed on an evenly-spaced, dense grid with volume element 0.005 Å^3. Previous calculations on PEN[24] found such a sampling to be sufficient for describing $\mathcal{F}(\mathbf{r})$. We expect a similar convergence behavior for TIPS-PEN because, like PEN, the frontier molecular orbitals that contribute to low-energy excitons are π-type states arising from linear combinations of C p_z orbitals.

3. Results and Discussion

3.1. Relating Polarization-Dependent Optical Absorption and Structure

Figure 2 compares the polarization-averaged measured and predicted optical absorption spectrum for crystalline TIPS-PEN, with the calculations averaged over the *ab* plane. As noted in the Experimental Section, TIPS-PEN molecules are expected to crystallize with the *ab* crystal plane parallel to the substrate and, therefore, incident light in the microscope will not couple

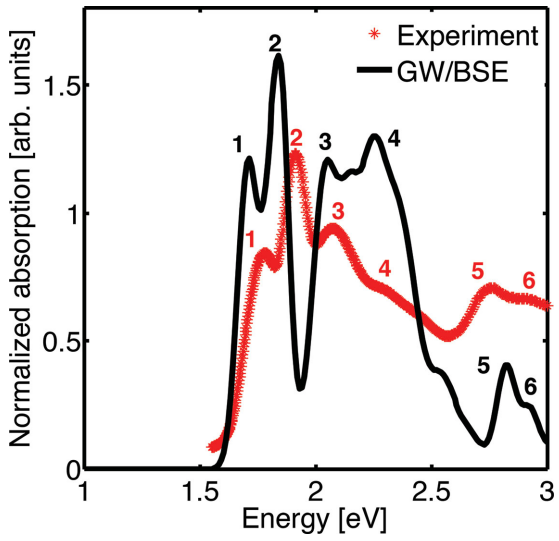

Figure 2. Comparison of the polarization-averaged optical absorption spectrum predicted for the bulk single crystal (black) and measured within a polycrystalline film (red), showing six distinct peaks in the absorption spectrum labeled 1–6 for both theory and experiment. The spectra are normalized such that the integral within the interval shown is 1. The calculated absorption spectrum is averaged over 18 polarizations within the *ab* crystalline plane (see text for details).

strongly to the [001] crystallographic axis. Within the visible region, there are three distinct and narrow low-energy peaks (labeled 1, 2, 3) in the measured spectrum at 1.8, 1.9, and 2.0 eV and three broad peaks (labeled 4, 5, 6) at ≈2.4, 2.8, and 2.9 eV. There is both qualitative and quantitative agreement of the computed spectrum with experiment in that all the peaks are predicted to be within 0.1 eV of experiment. However, there is some discrepancy of the predicted linewidth at higher energies. This may be due to a limited accuracy of the GW/BSE at energies above the fundamental gap or due to experimental conditions such as finite temperature effects.

Figure 3a shows the result of spatially-resolved optical absorption measurements on single domains within polycrystalline TIPS-PEN films. The measured optical absorption at 20° in Figure 3a clearly shows two nearby grains labeled domains 1 and 2. We find that the polarization-averaged absorption spectrum within these domains is nearly identical (see top panel of Figure 3b,c); the two adjacent domains can be distinguished only by polarization-angle-resolved absorption, suggesting their relative orientations are different. In this case, the orientations are approximately orthogonal, as determined by the angles of maximum absorption for the individual peaks in Figures 3b,c.

Figure 3d shows the predicted polarization-dependent absorption spectrum of TIPS-PEN, with the calculations restricted to the *ab* crystalline plane. Because the experimental angle is measured with respect to the lab frame, the relative angles between peaks and the breadth of their distribution can be compared to the calculation. We have plotted the predicted data to show the agreement visually with the measured data of Domain 2 in Figure 3c. We find excellent agreement between theory and experiment; Peak 1 strongly depends on the polarization, whereas Peak 2 is far less sensitive. The strong polarization-dependence of Peak 1 agrees with recently published measurements.[20]

Although one may expect that Peaks 2 and 3 are a vibronic progression of Peak 1, the weak polarization dependence of Peak 2, shown in Figures 3b,c, suggests that this peak is unlikely to be solely the result of vibronic progression. Our calculations confirm that there are contributions to these two peaks that correspond to distinct electronic transitions.

The polarization dependence of Peak 2 can be explained by means of further analysis of the computed variation of absorption for each contributing electronic transition. **Figure 4** shows the computed absorption as a function of polarization for the transition associated with the first singlet excited-state (S_1) that corresponds to Peak 1, and transitions associated with the three subsequent nearly-degenerate states (S_2-S_4) that make up Peak 2 (some peaks in the absorption are composed of multiple states, an issue elaborated below). For the S_1 transition, the absorption maximum is predicted to occur when light is polarized along the ~**-ab** direction (purple in Figure 4) and the minimum is predicted along ~**ab** (orange). Interestingly, the S_2 and S_3 transitions have this same polarization dependence, while S_4 is exactly out of phase, resulting in a weaker angle dependence for Peak 2. Therefore, each of the three individual transitions that spectrally overlap around 1.8 eV has a strong polarization-dependent absorption, while their combination does not.

Thus far, we have restricted our analysis to the *ab* crystallographic plane in order to compare with experiment. However, it is generally expected that the polarization-dependent

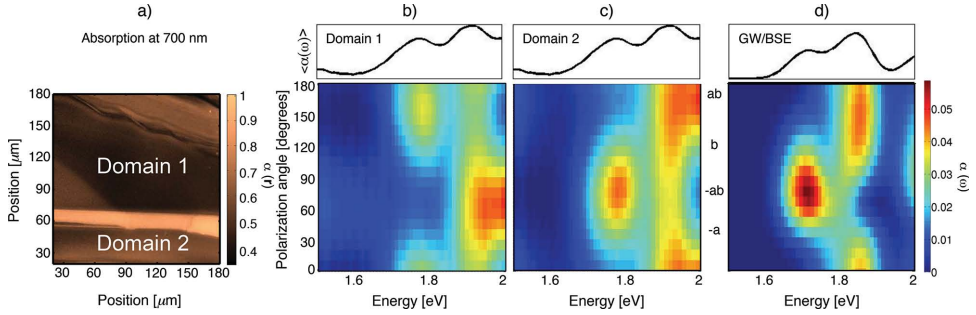

Figure 3. a) Measured spatially-resolved optical absorption at 700 nm within the TIPS-PEN polycrystalline thin film examined here, at 20° polarization within the lab frame. The two domains studied are labeled domain 1 and 2. Angle-dependence of optical absorption ($\alpha(\omega)$) within Domains b) 1 and c) 2 is compared to d) theory with the polarization averaged spectrum ($\langle\alpha(\omega)\rangle$) shown above each panel. The spectra in (b–d) are normalized such that the integral within the interval shown is 1.

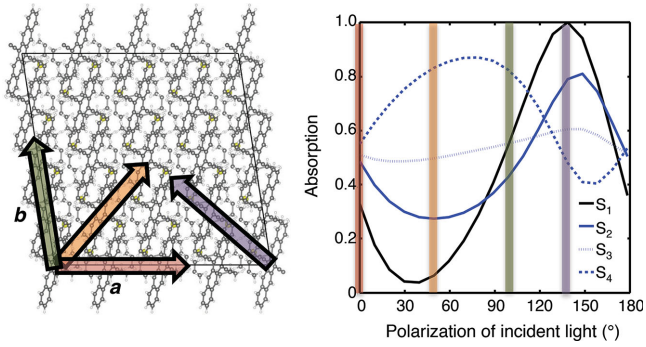

Figure 4. Calculated polarization depdendence of the first four optical transitions from GW/BSE (right), along with the crystal structure within the *ab* plane (left). Polarizations along **a** (0°), **b** (99.0°), **ab** (49.5°), and **-ab** (139.5°) are indicated with red, green, orange, and purple vertical bars, following the color-coded arrows on the left. State 1 makes up the first peak in absorption, while States 2-4 make up the second peak. The absorption is normalized by the maximum in Peak 1.

spectrum of the crystal follows that of the molecule and the molecular axes within the TIPS-PEN crystal are not confined to the *ab* plane. The short molecular axis of the PEN backbone, as defined in Figure 1, is directed along ≈(0.4, 0.7, 0.6) crystalline direction, and the long axis is along ≈(0.6, 0.8, –0.1). For the vectors within the *ab* crystalline plane that were considered above, the maximum overlap between the molecular short axis occurs at (–0.7, 0.6, 0) and the minimum at (0.5, 0.5, 0), consistent with the highest and lowest absorption strength, respectively. This suggests that the molecular axes do indeed play a role in the polarization-dependence of absorption.

Figure 5 shows the computed imaginary component of the dielectric function (ϵ_2) of both gas-phase molecule and crystal for light polarized along the short and long axes of the PEN backbone, along with a decomposition of the spectrum into the singlet excited-state transitions. For the gas-phase molecule, our calculated spectrum is composed of 3 transitions below 3.5 eV, which result in 3 peaks in ϵ_2 (with the second and third peaks

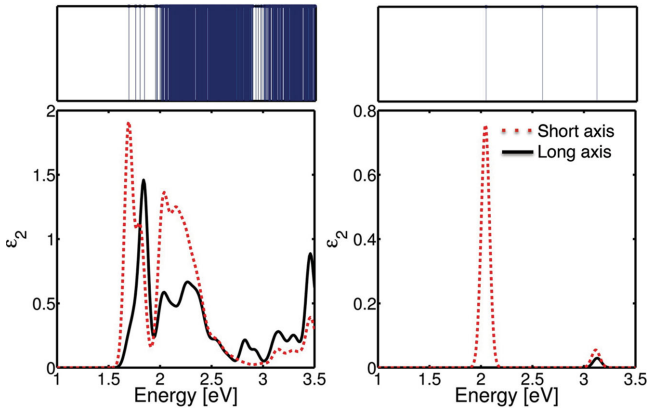

Figure 5. Imaginary component of the dielectric function (ϵ_2) of the isolated molecule (right) and bulk crystal (left), for light polarized along the short and long axes of the PEN backbone. The molecular axes are defined as in Figure 1, with the long axis along the aromatic backbone. The dielectric function is given in units of the vacuum permitivity, ϵ_0. The top panels show a line for each singlet excited-state transition that contributes to ϵ_2.

having very low intensity). The first two transitions are strongly coupled to light polarized along the short axis of the molecule, indicating that the transition dipole moments of these excited-states are also aligned with the short axis. The third transition couples equally strongly to light polarized in both directions.

In contrast to the gas-phase, all but the first peak in the solid-state spectrum are composed of multiple low-energy excited-state transitions. Within organic crystals, the long-range order and π-orbital overlap in the crystal result in the formation of many nearly-degenerate excited-state transitions.[41] Beyond 2 eV, we predict that a continuum of excited states contribute transitions to the crystal absorption spectrum. The first peak couples strongly to light polarized along the molecule's short axis, while higher energy peaks do not show this molecular nature.

In summary, our polarization-dependent studies suggest that it is important to treat the solid-state environment in order to understand the optoelectronic properties of organic crystals. For crystalline TIPS-PEN, while the polarization-dependent behavior of the first peak in the absorption spectrum does indeed follow that of the molecule, higher energy peaks deviate significantly from what would be predicted based on the molecule alone. The combination of predicted and measured angle-dependent absoprtion spectrum may be utilized for the determination of inter-grain orientation between arbitrary grains within a polycrystalline film.

3.2. Tuning Low-Energy Excitons by Solid-State Structure

The nature of the solid-state exciton and its degree of charge-transfer character can influence its propensity for SF and its diffusion properties throughout the crystal.[4] Here, we analyze the spatial distribution of low-energy singlet excitations within the TIPS-PEN crystal via the analysis presented in Equation 2. Such an analysis is important for understanding the behavior of excitons in crystals: the periodicity of the crystal and the symmetries associated with it allow the electron and hole to exist anywhere in the extended crystal; however, their relative motion is correlated. Equation 2 computes the probability of finding the electron and hole separated by some distance, **r**. It allows us to describe the distribution, extent, and degree of charge-transfer of a given exciton in terms of relative electron and hole coordinates.

As mentioned above, $\mathcal{F}(\mathbf{r})$ is the probability of finding an electron and hole separated by **r**. **Figure 6** presents $\mathcal{F}(\mathbf{x},\mathbf{y})$ and $\mathcal{F}(\mathbf{x},\mathbf{z})$, where the **z** and **y** axes are, respectively, integrated out of $\mathcal{F}$. The origin for both electron and hole is the same so that the point $\mathbf{r} = \mathbf{0}$ corresponds to electron and hole occupying the same coordinates. The exciton amplitude decays at long distances as shown in Figure 6a-d. Due to attractive Coulomb interactions between electron and hole, there is negligible probability that the distances between them will be very great. For S_1, within the *xy* plane, the high probability regions of $\mathcal{F}(\mathbf{x},\mathbf{y})$ for the lowest energy exciton extend over ~3 nm along the **y** axis, corresponding to a distribution over 3 molecules (Figure 6a). The exciton displays characteristics of charge-transfer, in that at the origin where electron and hole would have maximal overlap, the probability is suppressed compared to the amplitude of $\mathcal{F}(\mathbf{x},\mathbf{y})$ at the

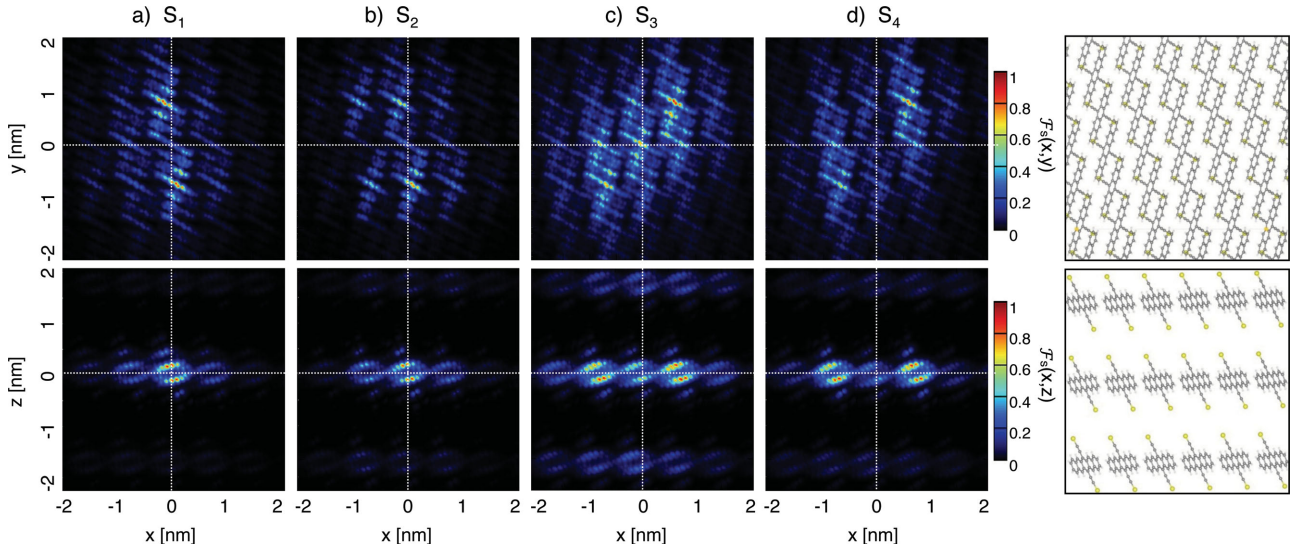

Figure 6. The predicted electron-hole correlation function for the first four excited-states within bulk TIPS-PEN (labeled States 1– 4 in Figure 4), projected onto the *xy* and *xz* planes, with the corresponding crystal orientation shown to the right. While the methyl side groups of the TIPS-PEN molecules are not shown in the schematic crystal drawing, they were included in the calculation.

coordinates (0,≈1 nm) and (0,≈–1 nm), which corresponds to the electron and hole occupying nearest neighbor molecules. Along the ***x*** axis, there is also a distribution of the exciton over ≈3 nm (over 3 molecules), though the probability is lower than along ***y***. There is no delocalization along the ***z*** axis, due to the large inter-molecular spacing introduced by the bulky functional groups along this axis, suggesting that the exciton is largely confined to the plane of the crystal parallel to the substrate.

For S_1, the exciton is quasi one-dimensional in that $\mathcal{F}(\mathbf{x},\mathbf{y})$ shows a strong preference for delocalization along the ***y***-axis. While S_2 is similar in nature to S_1 with slightly more delocalization, S_3 and S_4 are delocalized along nearest and next-nearest neighbors, as can be seen in Figure 6c,d. Our calculations were performed at zero temperature and it is possible that the excitons at room temperature are more localized. However, the exciton character, for example, direction and relative amount of delocalization among different singlet states is likely preserved.

The spatial anisotropy of the exciton can be understood by considering the high energy dispersion directions in the bandstructure,[42] which are determined from the π-orbital overlap. We compute the quasiparticle energies associated with valence and conduction states in TIPS-PEN along high symmetry directions in k-space using the GW approximation as shown in **Figure 7**. The large dispersion along the Z-N path is consistent with the lowest two excitons' delocalization along the crystal's ***b***-axis. On the other hand, the minimal dispersion from G to M (0, 0, 0.5) is consistent with the lack of exciton delocalization along the crystal's c-axis. Our calculations predict a large dispersion of the conduction band (0.8 eV) and smaller dispersion of the valence band (0.15 eV). These results are in good agreement with previous Hückel-model and DFT-based studies of the TIPS-PEN crystal.[17,18]

Our current study, along with prior work on other π-conjugated molecular crystals, indicates that the nature of excitons within organic crystals is strongly structure-dependent,[21–25,44–46] and is highly sensitive to π-orbital stacking. This suggests that the excitonic properties of TIPS-PEN can be modified for improved functionality because, as mentioned in Section 1, the inter-molecular arrangement of TIPS-PEN is highly tunable via changes in processing conditions.[7,10,11]

To gain further insight into the influence of inter-molecular packing on the nature of the exciton, we explore the variations in spatial profiles of the structure of a different PEN derivative, per-fluorinated PEN (PFP), where the molecules are in a face-to-face configuration.[47] Here, the nearest neighbor molecules are offset along the molecular short axis, in contrast to the TIPS-PEN structure where nearest neighbor molecules are offset along the long molecular axis. This structure (shown in

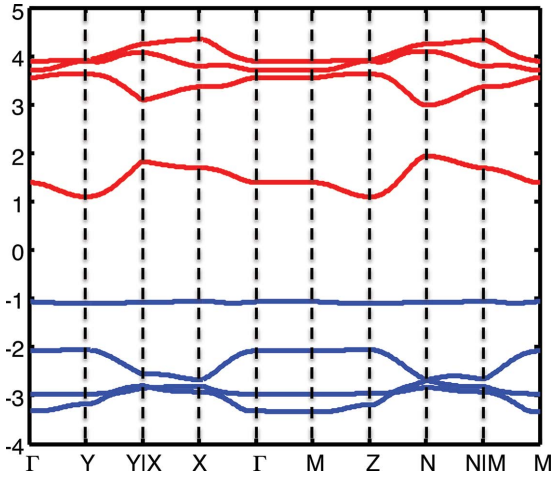

Figure 7. Computed bandstructure of the TIPS-PEN crystal. The valence states are shown in blue while the conduction states are in red. Zero defines the top of the valence band. The high symmetry points are defined following the convention found in another study.[43] The points Y|X and N|M are (0.475, 0.446, –0.099) and (–0.01, 0.473, 0.387) in reciprocal lattice coordinates, respectively. The highest dispersion direction in the bandstructure is the path from Z (–0.5, 0, 0.5) to N (–0.5, 0.5, 0.5).

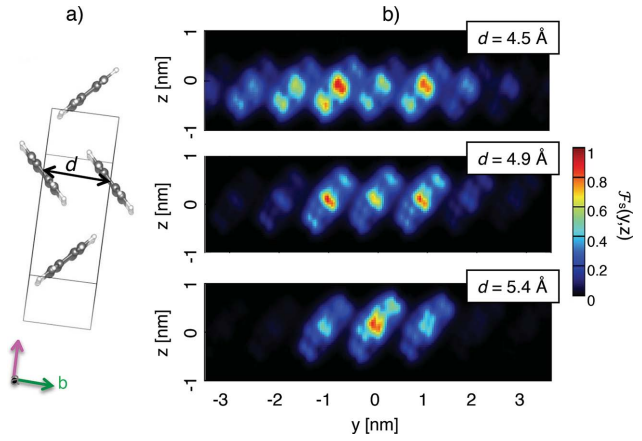

Figure 8. a) PEN molecule in a face-to-face structure. b) Electron-hole correlation function as the inter-molecular distance (labeled d) is varied from 4.5 Å through 4.95 Å and 5.4 Å.

Figure 8) is chosen because the π-orbital stacking is in one-dimension, allowing us to modify the π-orbital stacking distance between two neighboring molecules in our calculations by straightforward isotropic change of the crystal volume. PEN molecules are placed in the crystal structure of PFP and the unit cell vectors are set to 1.0, 1.1, and 1.2 times that of PFP, resulting in an intermolecular separation of 4.5 Å, 4.95 Å, and 5.4 Å, respectively and π-orbital stacking distance (defined as the shortest distance between two nearest neighbor molecule) of 3.2 Å, 3.5 Å, and 3.8 Å, respectively.[48]

As shown in Figure 8, the lowest energy exciton for PEN in this PFP lattice has a one-dimensional character, consistent with the direction of π-orbital overlap; and the delocalization is highly dependent on inter-molecular distance. As the inter-molecular distance is increased from 4.5 Å to 4.95 Å and 5.4 Å, the exciton delocalizes over 7, 5, and 3 molecules, respectively. This result suggests that the exciton delocalization for PEN derivatives is significantly affected by the solid-state structure.

PEN derivatives are of particular interest for organic photovoltaics because they undergo SF, which is thought to occur in part because it is either a resonant process, i.e., the energy of the lowest energy singlet is roughly equal to twice that of the triplet or that any excess energy from downconversion is able to be dissipated in the lattice. [13,14,49–52] Additionally, it is expected that either the optically excited state has a charge-transfer character or that there exists an intermediate charge-transfer state to mediate SF.[4] Recent measurements on PFP suggest that π-orbital overlap is also necessary for efficient SF.[46]

Table 1 shows the calculated singlet and triplet energies for TIPS-PEN and the PEN in the PFP structures studied in this work. For TIPS-PEN, we find that it is energetically neutral to convert one singlet to two triplets, consistent with recent observations of SF.[15,26,53] For the three PEN-in-PFP structures studies, SF is either energetically neutral or favorable. As the inter-molecular spacing is increased for PEN-in-PFP, the SF process becomes more energetically favorable (i.e., S_1-$2T_1$ increases). However, as the inter-molecular spacing increases, the predicted degree of charge-transfer decreases, which is believed to be less favorable for SF. The loss of charge-transfer character is visually apparent in Figure 8 and can be quantified

Table 1. Computed GW/BSE lowest singlet (S_1) and triplet (T_1) energies, as well as the energy difference between one singlet and two triplets, in eV, in TIPS-PEN and in face-to-face ordered PEN (PEN-in-PFP) with variable inter-molecular distance given in parentheses.

	S_1	T_1	$S_1 - 2T_1$
TIPS-PEN	1.7	0.85	0.0
PEN-in-PFP (4.5 Å)	1.0	0.5	0.0
PEN-in-PFP (4.95 Å)	1.7	0.7	0.3
PEN-in-PFP (5.4 Å)	2.1	0.8	0.5

by a simple estimate of the degree of charge-transfer. We calculate this quantity as the percentage of $\mathcal{F}(r)$ contained within a volume corresponding to one molecule.[24] Within this approximation, the degree of charge-transfer of the lowest energy exciton varies between 57% at 4.5 Å to 24% at 5.4 Å separation for the face-to-face ordered PEN crystals studied here.

As noted in previous studies,[24,25] there are competing energy scales that modify the character of the exciton: electron-hole Coulomb-like interactions localize the exciton; π-orbital overlap delocalizes the exciton; and repulsive exchange induces charge-transfer. As the inter-molecular distance increases, the exciton tends to localize because of the poor π-orbital overlap, concomitantly suppressing charge-transfer character. Because the degree of charge-transfer character has been connected to the efficiency of SF,[4] our calculations suggest that morphological control could be used to tune SF in organic crystals. In particular, the tunablility of the inter-molecular structure of TIPS-PEN should allow for optimization of its SF efficiency via the solid-state. The relationship between solid-state morphology and singlet fission efficiency has been recently noted in several studies. [13,46,54,55]

3.3. Gap Renormalization and Physical Structure

Lastly, we address the difference in solid-state polarization between PEN and TIPS-PEN, which has been recently measured and calculated.[19,56,57] **Table 2** presents the computed TIPS-PEN gas-phase and bulk crystalline fundamental gap, that is, the electron addition-removal gap. The gas-phase gap (which is equal to the difference between the molecule's ionization energy and electron affinity) of 4.0 eV in TIPS-PEN is 0.5 eV smaller than the 4.5 eV predicted for PEN within the same level of theory.[23] This can be explained*f* by the additional delocalization of molecular orbitals along the C-C triple bond of the side group. In the crystalline TIPS-PEN, the fundamental gap is also slightly smaller than predicted for PEN (by 0.1 eV).

It is well understood that the energy to add or remove an electron from a molecule decreases when the molecule is in a

Table 2. Computed GW fundamental gaps for TIPS-PEN and PEN in the gas- and crystalline- phase, in eV.

	TIPS-PEN	PEN[23]
Gas-phase	4.0	4.5
Crystal	2.1	2.2

polarizable environment, leading to energy level renormalization and reduction of the fundamental gap.[58] It is also well-known that this effect is well-captured by the GW approximation.[59,60] When compared with the gas-phase, the solid-state ionization energy will be reduced and the electron affinity increased, respectively, by the energy of electronic polarization upon injection of a positive charge (P_+) or negative charge (P_-) into the crystal. If for simplicity, we assume that $P_+ \sim P_- \sim P$, the solid-state gap, E^{sol}, is then determined from the gas-phase gap, E^{mol}, as $E^{sol} = E^{mol} - 2P$. Here, the value of P extracted from GW is 0.95 eV for TIPS-PEN, which is 0.2 eV smaller than a similar level of theory predicts for PEN.[23]

The reduction of solid-state polarization upon functionalization in TIPS-PEN can be understood from the increased inter-molecular separation compared to the PEN crystal. Recent measurement of P_+ suggest that this value is larger in TIPS-PEN than in PEN by 0.25 eV for crystals and 0.4 eV for more amorphous structures,[56,57] in good agreement with our prediction of 0.2 eV and a recently predicted value of 0.4 eV.[19]

4. Conclusions

In summary, we have combined spatially-resolved optical absorption measurement with the first ab initio excited-state calculations of solid-state TIPS-PEN, a promising candidate organic optoelectronic material, in order to understand the relationship between its optical absorption properties and solid-state structure. Angle-dependent optical absorption measurements and calculations were used to understand the strong dependence of absorption strength on the polarization of incident light, and to understand the deviation of polarization angle-dependence from that of the isolated molecule. We demonstrated that a combination of ab initio theory and experiment can be utilized to determine the exact relative orientation between different grains of polycrystalline thin films and to understand the role of relative domain orientation in the behavior of excitons. Additionally, we determined that the lowest energy exciton in the bulk is delocalized, extending over nearest neighbor molecules within the crystal (≈3 nm), and is contained within the *ab* crystallographic plane. We predict that the properties directly applicable to singlet fission—singlet-triplet energy splitting and the degree of delocalization and charge-transfer character of the singlet exciton—are highly tunable via change in π-orbital stacking, suggesting that solid-state structure can be tailored to optimize singlet fission with suitable functionalization or growth conditions.

Acknowledgments

The authors thank Pierre Darancet (Argonne National Laboratory) for valuable discussions. Work at the Molecular Foundry was supported by the Office of Science, Office of Basic Energy Sciences, of the U.S. Department of Energy under Contract DE-AC02-05CH11231. Partial support for this work was also provided through Scientific Discovery through Advanced Computing (SciDAC) Partnership program funded by U.S. Department of Energy, Office of Science, Advanced Scientific Computing Research and Basic Energy Sciences. Experimental work was supported by the Defense Advanced Research Projects Agency Young Faculty Award number N66001-12-1-4228. N.S.G. thanks the David and Lucile Packard Foundation Fellowship for Science and Engineering. C.Y.W. thanks the Natural Sciences and Engineering Research Council, Canada, for a Postdoctoral Fellowship. B.L.C. acknowledges a National Science Foundation Graduate Research Fellowship (DGE 1106400). Work at the Weizmann Institute of Science was additionally supported by the Israel Science Foundation, the Helmsley Foundation, the Wolfson Foundation, and the Lise Meitner Minerva Center for Computational Chemistry. The authors also acknowledge funding from the United States-Israel Binational Science Foundation (BSF). The authors thank the National Energy Research Scientific Computing (NERSC) center, which is supported by the Office of Science of the U.S. Department of Energy under Contract DE-AC02-05CH11231, and the Argonne Leadership Computing Facility for computational resources, which is supported by the Office of Science of the U.S. Department of Energy under Contract DE-AC02-06CH11357.

Received: August 31, 2014
Revised: November 3, 2014
Published online: December 6, 2014

[1] J. E. Anthony, *Angew. Chem. Int. Ed.* **2008**, *47*, 452.
[2] J. E. Anthony, *Chem. Rev.* **2006**, *106*, 5028.
[3] A. D. Platt, J. Day, S. Subramanian, J. E. Anthony, O. Ostroverkhova, *J. Phys. Chem. C* **2009**, *113*, 14006.
[4] M. B. Smith, J. Michl, *Chem. Rev.* **2010**, *110*, 6891.
[5] D. N. Congreve, J. Lee, N. J. Thompson, E. Hontz, S. R. Yost, P. D. Reusswig, M. E. Bahlke, S. Reineke, T. Van Voorhis, M. A. Baldo, *Science* **2013**, *340*, 334.
[6] O. Ostroverkhova, S. Shcherbyna, D. G. Cooke, R. F. Egerton, F. A. Hegmann, R. R. Tykwinski, S. R. Parkin, J. E. Anthony, *J. Appl. Phys.* **2005**, *98*, 033701.
[7] J. E. Anthony, J. S. Brooks, D. L. Eaton, S. R. Parkin, *J. Am. Chem. Soc.* **2001**, *123*, 9482.
[8] S. K. Park, T. N. Jackson, J. E. Anthony, D. A. Mourey, *Appl. Phys. Lett.* **2007**, *91*, 063514.
[9] A. Maliakal, K. Raghavachari, H. Katz, E. Chandross, T. Siegrist, *Chem. Mater.* **2004**, *16*, 4980.
[10] G. Giri, E. Verploegen, S. C. B. Mannsfeld, S. Atahan-Evrenk, D. H. Kim, S. Y. Lee, H. A. Becerril, A. Aspuru-Guzik, M. F. Toney, Z. Bao, *Nature* **2011**, *480*, 505.
[11] J. Xu, Y. Diao, D. Zhou, Y. Mao, G. Giri, W. Chen, N. Liu, S. C. B. Mannsfeld, G. Xue, Z. Bao, *J. Mater. Chem. C* **2014**, *2*, 2985.
[12] Sam L. Bayliss, Alexei D. Chepelianskii, Alessandro Sepe, Brian J. Walker, Bruno Ehrler, Matthew J. Bruzek, John E. Anthony, Neil C. Greenham, *Phys. Rev. Lett.* **2014**, *112,* 238701.
[13] S. R. Yost, J. Lee, M. W. B. Wilson, T. Wu, D. P. McMahon, R. R. Parkhurst, N. J. Thompson, D. N. Congreve, A. Rao, K. Johnson, M. Y. Sfeir, M. G. Bawendi, T. M. Swager, R. H. Friend, M. A. Baldo, T. Van Voorhis, *Nat. Chem.* **2014**, *6*, 492.
[14] J. C. Johnson, A. J. Nozik, J. Michl, *Acc. Chem. Res.* **2013**, *46*, 1290.
[15] C. Ramanan, A. L. Smeigh, J. E. Anthony, T. J. Marks, M. R. Wasielewski, *J. Am. Chem. Soc.* **2012**, *134*, 386.
[16] R. B. Campbell, J. M. Robertson, J. Trotter, *Acta Crystal.* **1962**, *15*, 289.
[17] R. C. Haddon, X. Chi, M. E. Itkis, J. E. Anthony, D. L. Eaton, T. Siegrist, C. C. Mattheus, T. T. M. Palstra, *J. Phys. Chem. B* **2002**, *106*, 8288.
[18] A. Troisi, G. Orlandi, J. E. Anthony, *Chem. Mater.* **2005**, *17*, 5024.
[19] S. M. Ryno, C. Risko, J.-L. Bredas, *J. Am. Chem. Soc.* **2014**, *136*, 6421.
[20] D. T. James, J. M. Frost, J. Wade, J. Nelson, J.-S. Kim, *ACS Nano* **2013**, *7*, 7983.

[21] M. L. Tiago, J. E. Northrup, S. G. Louie, *Phys. Rev. B* **2003**, *67*, 115212.
[22] C. Ambrosch-Draxl, D. Nabok, P. Puschnig, C. Meisenbichler, *New J. Phys.* **2009**, *11*, 125010.
[23] S. Sharifzadeh, A. Biller, L. Kronik, J. B. Neaton, *Phys. Rev. B* **2012**, *85*, 125307.
[24] S. Sharifzadeh, P. Darancet, L. Kronik, J. B. Neaton, *J. Phys. Chem. Lett.* **2013**, *4*, 2197.
[25] P. Cudazzo, M. Gatti, A. Rubio, *Phys. Rev. B* **2012**, *86*, 195307.
[26] C. Y. Wong, S. B. Penwell, B. L. Cotts, R. Noriega, H. Wu, N. S. Ginsberg, *J. Phys. Chem. C* **2013**, *117*, 22111.
[27] J. Deslippe, G. Samsonidze, D. A. Strubbe, M. Jain, M. L. Cohen, S. G. Louie, *Comp. Phys. Commun.* **2012**, *183*, 1269.
[28] M. S. Hybertsen, S. G. Louie, *Phys. Rev. B* **1986**, *34*, 5390.
[29] J. P. Perdew, K. Burke, M. Ernzerhof, *Phys. Rev. Lett.* **1996**, *77*, 3865.
[30] M. Rohlfing, S. G. Louie, *Phys. Rev. B* **2000**, *62*, 4927.
[31] P. Giannozzi, S. Baroni, N. Bonini, M. Calandra, R. Car, C. Cavazzoni, D. Ceresoli, G. L. Chiarotti, M. Cococcioni, I. Dabo, A. D. Corso, S. de Gironcoli, S. Fabris, G. Fratesi, R. Gebauer, U. Gerstmann, C. Gougoussis, A. Kokalj, M. Lazzeri, L. Martin-Samos, N. Marzari, F. Mauri, R. Mazzarello, S. Paolini, A. Pasquarello, L. Paulatto, C. Sbraccia, S. Scandolo, G. Sclauzero, A. P. Seitsonen, A. Smogunov, P. Umari, R. M. Wentzcovitch, *J. Phys,: Condens. Matter* **2009**, *21*, 395502.
[32] N. Troullier, J. L. Martins, *Phys. Rev. B* **1991**, *43*, 1993.
[33] D. Corso, Http://theossrv1.epfl.ch/Main/Pseudopotentials.
[34] S. C. B. Mannsfeld, M. L. Tang, Z. Bao, *Adv. Mater.* **2011**, *23*, 127.
[35] G. Grosso, G. Parravicini, *Solid State Physics*, 2nd Ed. Academic Press, London **2003**.
[36] Previous attempts to visualize exciton delocalization in periodic structures have relied on equivalent quantities within semi-empirical methods (Ref. 37) or time-dependent DFT (Ref. 38).
[37] L. Romaner, G. Heimel, H. Wiesenhofer, P. Scandiucci de Freitas, U. Scherf, J.-L. Brédas, E. Zojer, E. J. W. List, *Chem. Mater.* **2004**, *16*, 4667.
[38] S. Tretiak, K. Igumenshchev, V. Chernyak, *Phys. Rev. B* **2005**, *71*, 033201.
[39] P. Petelenz, B. Pac, *J. Am. Chem. Soc.* **2013**, *135*, 17379.
[40] J. Chen, D. C. Martin, J. E. Anthony, *J. Mater. Res.* **2007**, *22*, 1701.
[41] C. J. Bardeen, *MRS Bull.* **2013**, *38*, 65.
[42] J. L. Bredas, J. P. Calbert, D. A. da Silva Filho, J. Cornil, *Proc. Natl. Acad. Sci.* **2002**, *99*, 5804.
[43] S. Curtarolo, W. Setyawan, G. L. Hart, M. Jahnatek, R. V. Chepulskii, R. H. Taylor, S. Wang, J. Xue, K. Yang, O. Levy, M. J. Mehl, H. T. Stokes, D. O. Demchenko, D. Morgan, *Comput. Mater. Sci.* **2012**, *58*, 218.
[44] F. Roth, B. Mahns, S. Hampel, M. Nohr, H. Berger, B. Buchner, M. Knupfer, *Euro. Phys. J. B* **2013**, *86*, 66.
[45] F. Roth, P. Cudazzo, B. Mahns, M. Gatti, J. Bauer, S. Hampel, M. Nohr, H. Berger, M. Knupfer, A. Rubio, *New J. Phys.* **2013**, *15*, 125024.
[46] K. Kolata, T. Breuer, G. Witte, S. Chatterjee, *ACS Nano* **2014**, *8*, 7377.
[47] Y. Sakamoto, T. Suzuki, M. Kobayashi, Y. Gao, Y. Fukai, Y. Inoue, F. Sato, S. Tokito, *J. Am. Chem. Soc.* **2004**, *126*, 8138.
[48] GW calculations are performed with 704, 774, and 846 unoccupied states for inter-molecular separations of 4.5Å, 4.9Å, and 5.1Å, respectively. The BSE sum is computed with 12 occupied and 12 unoccupied bands and expanded in a supercell of $6 \times 12 \times 6$ primitive cells.
[49] V. K. Thorsmolle, R. D. Averitt, J. Demsar, D. L. Smith, S. Tretiak, R. L. Martin, X. Chi, B. K. Crone, A. P. Ramirez, A. J. Taylor, *Phys. Rev. Lett.* **2009**, *102*, 017401.
[50] W.-L. Chan, M. Ligges, A. Jailaubekov, L. Kaake, L. Miaja-Avila, X.-Y. Zhu, *Science* **2011**, *334*, 1541.
[51] W.-L. Chan, T. C. Berkelbach, M. R. Provorse, N. R. Monahan, J. R. Tritsch, M. S. Hybertsen, D. R. Reichman, J. Gao, X.-Y. Zhu, *Acct. Chem. Res.* **2013**, *46*, 1321.
[52] A. B. Kolomeisky, X. Feng, A. I. Krylov, *J. Phys. Chem. C* **2014**, *118*, 5188.
[53] B. J. Walker, A. J. Musser, D. Beljonne, R. H. Friend, *Nat. Chem.* **2013**, *5*, 1019.
[54] L. Wang, Y. Olivier, O. V. Prezhdo, D. Beljonne, *J. Phys. Chem. Lett.* **2014**, *5*, 19, 3345.
[55] X. Feng, A. B. Kolomeisky, A. I. Krylov, *J. Phys. Chem. C* **2014**, *118*, 34, 19608.
[56] O. L. Griffith, J. E. Anthony, A. G. Jones, D. L. Lichtenberger, *J. Am. Chem. Soc.* **2010**, *132*, 580.
[57] Y. Qi, S. K. Mohapatra, S. B. Kim, S. Barlow, S. R. Marder, A. Kahn, *Appl. Phys. Lett.* **2012**, *100*, 083305.
[58] N. Sato, H. Inokuchi, E. A. Silinsh, *Chem. Phys.* **1987**, *115*, 269.
[59] J. B. Neaton, M. S. Hybertsen, S. G. Louie, *Phys. Rev. Lett.* **2006**, *97*, 216405.
[60] S. Refaely-Abramson, S. Sharifzadeh, M. Jain, R. Baer, J. B. Neaton, L. Kronik, *Phys. Rev. B* **2013**, *88*, 081204.